Hidden hysteretic behavior of a paramagnetic iron(II) network revealed by light irradiation

Mame Mguenar Ndiaye, Sébastien Pillet, El-Eulmi Bendeif, Mathieu Marchivie, Guillaume Chastanet, Kamel Boukheddaden, Smail Triki

DOI: 10.1002/ejic.200((will be filled in by the editorial staff))

Hidden Hysteretic Behavior of a Paramagnetic Fe(II) Network Revealed by Light Irradiation

Mame Mguenar Ndiaye[a], Sébastien Pillet[b], El-Eulmi Bendeif[b], Mathieu Marchivie[c],*, Guillaume Chastanet[c],*, Kamel Boukheddaden[d], Smail Triki[a],*

Keywords: Coordination Chemistry / Iron(II) / Spin-Crossover / LIESST / Photomagnetism / Hidden hysteresis / Elastic frustration

Abstract: The paramagnetic coordination polymer [Fe(3phOH-trz){Pt(CN)$_4$}].2H$_2$O was obtained by reaction of iron(II) salt with the 4-(3-hydroxyphenyl)-1,2,4-triazole (3phOH-trz) ligand and a [Pt(CN)$_4$]$^{2-}$ salt. Its structure consists in two dimensional {FePt(CN)$_4$} layers linked by π-stacking interactions and a strong H-bonds network between water molecules and the hydroxyl group from the ligand. From the paramagnetic high spin (HS) state at 10 K, irradiation at 830 nm led to the fully low spin (LS) state, according to the reverse-LIESST process. Upon warming, this LS state undergoes a thermally induced spin transition to high spin around 105 K. This photoswitching process is reversible and the paramagnetic state can be recovered by a 510 nm light irradiation below 105 K. Moreover, a permanent irradiation (830 nm) revealed a hidden hysteresis loop of 37 K width. Photocrystallographic experiments did not evidence any structural phase transition upon excitation but underlined that the elastic frustration might be responsible for the inhibition of the spin crossover in this compound and allowed the observation of the hidden hysteresis loop.

Introduction

Switching phenomenon of molecular based compounds is an open challenge for synthetic chemists worldwide.[1-3] In this context, photo-switching is under specific attention since it offers ultrafast (down to femtosecond) manipulation of physical properties.[4-6] Among a wide range of systems under investigation, materials that undergo a spin switching, whereby the central metal ion changes its spin state upon an external perturbation, have received considerable interest because of their potential applications as functional materials.[7,8] In this context, spin-crossover (SCO) complexes of 3d^4 to 3d^7 metal ions, displaying high-spin (HS) ↔ low-spin (LS) transition upon temperature, light, pressure, chemical or magnetic field perturbations, have focused a huge amount of investigations in the last 80 years because of potential involvement in optical switches or/and magneto-optical storage properties.[3,7-11] Most of the explored systems are pseudo-octahedral 3d^6 iron(II) complexes that may be either paramagnetic (HS, S = 2) or diamagnetic (LS, S = 0).

The photoswitching of SCO materials is mainly based on three different effects. The first one is related to an irradiation centered on photosensitive ligands such as photo-isomerizable units.[12] This effect, named LD-LISC for Ligand-Driven Light-Induced Spin Change, has been improved to be efficient at room temperature[13] but hardly works in the solid state due to strong steric hindrance. The second way of switching by light is based on photo-thermal effects: a pulsed laser irradiation from the LS state inside the thermal hysteresis loop induces enough local and fast heating to trigger the LS to HS spin transition in few nanoseconds.[14] This effect deserves a specific optical set up for ultrafast excitations and its reversibility is still debated.[15] A third strategy for the light-induced SCO is to use light excitation centered on the metal ions, a phenomenon known as Light-Induced Excited Spin State Trapping or LIESST effect[16] and observed on a large number of compounds. One of the main issue of this effect is related to the lifetime of the photo-induced state which has focused a large amount of work to understand the physical and chemical parameters allowing its improvement.[17,18] Basically, the higher the thermal spin-crossover temperature $T_{1/2}$ the faster the relaxation: a behavior that can be easily understood since the transition temperature $T_{1/2}$ is proportional to the strength of the ligand field, which stabilizes (resp. destabilizes) the LS (resp. HS) state. The first important parameter that was identified to increase the lifetime of the photo-induced state was the metal-ligand bond-length distance variation upon the spin-crossover: a huge variation increases the vibronic elastic energy barrier of the metastable HS state which then slows down its thermal relaxation.

Using the T(LIESST) measurement, which aims to estimate the limiting temperature above which the photoinduced HS metastable state is erased,[19] a [T(LIESST), $T_{1/2}$] database was built.[20] From this comparison of more than 50 compounds, the coordination sphere distortion was pointed as a crucial parameter to increase the lifetime of the photo-induced state. This has allowed to increase the T(LIESST) value from 60 K in the late 90's to 130 K for a pure iron(II) SCO material[21] and even 180 K in Prussian Blue analogues.[22]

[a] Mame Nguenar Ndiaye, Smail Triki, *UMR CNRS 6521, Univ. Brest (UBO), C.S. 93837 - 29238 Brest Cedex 3 – France ; smail.triki@univ-brest.fr*
[b] Sébastien Pillet and El-Eulmi Bendeif, *Université de Lorraine, CNRS, CRM2, Blvd des aiguillettes, 54506, Vandœuvre-lès-Nancy, France.*
[c] Mathieu Marchivie and Guillaume Chastanet, *CNRS, Université de Bordeaux, ICMCB, 87 avenue du Dr. A. Schweitzer, Pessac, F-33608, France,* guillaume.chastanet@icmcb.cnrs.fr ; mathieu.marchivie@icmcb.cnrs.fr
[d] Kamel Boukheddaden, *UMR-CNRS 8635, Univ. Versailles, 45 Av. des Etats-Unis 78035 Versailles, France.*

Supporting information for this article is available on the WWW under http://www.eurjic.org/ or from the author.

To circumvent the problem of the photo-induced state's lifetime, a new strategy has recently emerged. By taking advantage of the reversibility of the LIESST effect, [23] purely HS compounds can be converted at very low temperature into the LS state, and further undergo a LS to HS crossover while warming. In such cases, this implies that a hysteresis loop is hidden and can only be revealed by light irradiation. Since the hysteresis is due to a collective effect, the photo-induced states are stable.

There are two strategies to obtain such a hidden hysteresis loop. The first one aims at favoring the overlap between the T(LIESST) and the thermal hysteresis loop through metal dilution.[24] This has led to the observation of a light induced phase collapse on Prussian blue analogs.[25] The second strategy is based on elastic frustration, resulting from a competition between ferroelastic like (cooperativity-rigidity) and antiferroelastic like (flexibility) interactions, that can inhibit partially or completely the SCO.[26] With such strategy, the photoswitching efficiency can be improved and symmetry breaking can be promoted.[27] In this context, as a part of our and others ongoing work on the cooperative polynuclear or extended systems based on functionalized triazole ligands,[28-30] we have reported recently an original bidirectional photoswitching of a frustrated state.[30] Indeed, in the 2D [Fe(2-pytrz){Pt(CN)$_4$}].3H$_2$O network, **1**, (2-pytrz = 4-(2-pyridyl)-1,2,4-triazole), an intermediate HS-LS state is trapped at low temperature due to elastic strains. From this state the fully LS-LS or HS-HS states can be reached by irradiation at 830 nm and 510 nm, respectively. Moreover, a hidden hysteresis loop was evidenced by permanent light irradiation at 830 nm between the HS-LS and LS-LS states.[30]

To use such strategy, materials exhibiting reverse-LIESST effect are more suitable. This makes the Hoffman phase analogs very promising. Indeed, such systems can be highly functionalized to tune the rigidity/flexibility competition[31-34] and to exhibit LIESST and reverse-LIESST effects.[29a,31] In that sense, we present here as a continuation of our work on such systems[30] a new paramagnetic Hofmann-like phase that does not exhibit any thermal spin crossover. Using the reverse-LIESST approach we have evidenced the hidden hysteresis loop from a purely HS to a purely LS state. From low temperature photo-crystallography we have correlated this observation to the evolution of the structure under light irradiation.

Results and Discussion

Synthetic strategy.

From our previous work on [Fe(2-pytrz){Pt(CN)$_4$}].3H$_2$O network **1**,[30] we have shown that its structural topology consists of two dimensional {FePt(CN)$_4$} sheets connected to each other by strong hydrogen bonds mediated by three non-coordinated water molecules. In this particular system, the 2D sheets are corrugated due to the presence of two different iron(II) sites and the water molecules are mainly organized around only one of these sites. From crystallographic analysis, we have shown that this iron(II) ion does not exhibit any SCO and remains trapped in the HS state. It appeared that this site was the most constrained site. However, this HS ion was converted into its LS state by irradiation with near-infrared light through the reverse-LIESST effect, evidencing the occurrence of a hidden hysteresis loop.

Following this concept, we propose that favoring and strengthening the hydrogen bonding network would possibly end up with a fully constrained network and a purely HS material that can be erased using the reverse-LIESST effect. For that purpose, we have designed a new triazole-based ligand possessing a hydroxyl group to promote hydrogen bonds with water molecules. This approach has been previously used to strengthen the hydrogen bonding network using *saltrz* ligand ((E)-2-(((4H-1,2,4-triazol-4-yl)imino)methyl)phenol).[29a] This ligand connects a phenol ring to a triazole moiety by an imine function. In order to have a shorter connection between the phenol and the triazole and to enhance the rigidity of the ligand, the 4-(3-hydroxyphenyl)-1,2,4-triazole (3phOH-trz, scheme 1)) was synthesized as described in the experimental section. Small colorless square crystals of the [Fe(3phOH-trz){Pt(CN)$_4$}].2H$_2$O (**2**) were obtained by slow diffusion. Except the bands attributed to the [Pt(CN)$_4$]$^{2-}$ anion (Figure S1 and S4), the IR spectrum of the title compound is similar to that measured for the free 3phOH-trz ligand. The blue shift of the characteristic intense C=N stretching band ν_{CN} observed at 2169 cm^{-1}, which was located at 2133 and 2122 cm^{-1} in K$_2$[Pt(CN)$_4$].xH$_2$O, suggests the μ_4-bridging coordination mode of the [Pt(CN)$_4$]$^{2-}$ moiety. Moreover, the ν_{CN} bands of the free triazole unit, observed at 1598 and 1202 cm^{-1}, are shifted to 1599 and 1211 cm^{-1} in **2**, indicating its coordination to the Fe(II).

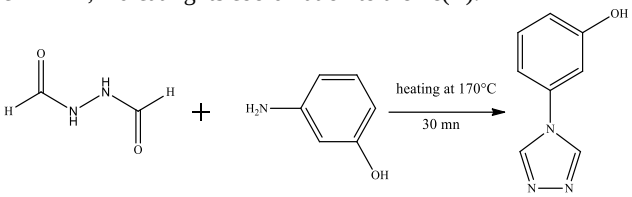

Scheme 1: synthesis of the 4-(3-hydroxyphenyl)-1,2,4-triazole.

Structural investigations.

The crystal structure of **2** was solved and refined firstly at 296 K and 110 K then, according to the photomagnetic properties, complementary photo-crystallography was performed at 10 K. The light induced structural behaviour will be detailed in the following paragraphs.

Compound **2** crystallizes in the monoclinic P2$_1$/c space group. Crystallographic data and the structural parameters of the FeN$_6$ octahedron are listed in Tables 1 and 2, respectively. The crystal structure is built from one Fe(II) site and one half [Pt(CN)$_4$]$^{2-}$ anion both located on an inversion center at (½, 0, ½) and (0, ½, ½), respectively. One monodentate 3phOH-trz ligand and one water molecule, both located on general positions, complete the crystal structure (Figure 1).

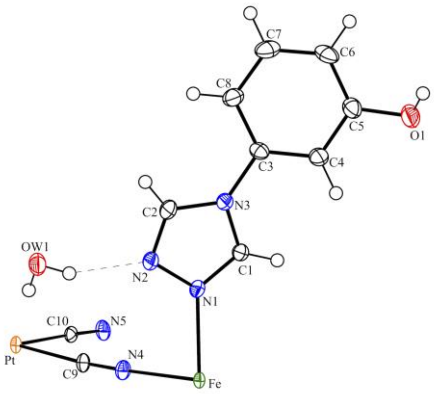

Figure 1. Thermal ellipsoid drawing (30% probability ellipsoids) of the asymmetric unit of **2** at 296 K showing the labeling scheme.

Table 1. Crystallographic data for compound **2**

	HS	HS	HS	LS
T / K	**296**	**110**	**10**	**10**
Color	**colorless**	**colorless**	**colorless**	**pink**
[a]Chemical formula	$C_{20}H_{18}FeN_{10}O_4Pt$	$C_{20}H_{18}FeN_{10}O_4Pt$	$C_{20}H_{18}FeN_{10}O_4Pt$	$C_{20}H_{18}FeN_{10}O_4Pt$
Formula weight	713.38	713.38	713.38	713.38
Crystal system	Monoclinic	Monoclinic	Monoclinic	Monoclinic
Space group	$P2_1/c$	$P2_1/c$	$P2_1/c$	$P2_1/c$
a/Å	7.6149(2)	7.6230(2)	7.6326(3)	7.4562(3)
b/Å	7.3105(2)	7.2775(2)	7.2627(3)	6.8994(3)
c/Å	22.3832(7)	22.2303(9)	22.1577(9)	22.1699(9)
β/°	98.137(3)	98.048(3)	98.071(4)	99.107(4)
Volume/Å^3	1233.5(1)	1221.1(1)	1216.1(1)	1126.1(1)
Z	2	2	2	2
ρ_{calc} g/cm^3	1.921	1.946	1.954	2.110
[b]Final R indexes	R_1 = 0.0204, wR_2 = 0.0392	R_1 = 0.0376, wR_2 = 0.0726	R_1 = 0.0295, wR_2 = 0.0609	R_1 = 0.027, wR_2 = 0.0602
[c]G.O.F on F^2	1.110	1.179	1.216	1.252

[a]There is 1/2 chemical formula in the asymmetric unit. [b]R1 = Σ(|Fo-Fc|/Fo) [I>=2σ (I)] and wR2 = [Σ((ω(Fo^2-Fc^2))^2/(ω(Fo^2))^2)]$^{1/2}$ [all data]. [c]G.O.F = [(Σ(ω(Fo^2-Fc^2))^2/(Nobs-Nvar)]$^{1/2}$

The iron centers are linked by $[Pt(CN)_4]^{2-}$ anions to form a 2-D coordination polymer within slightly corrugated layers corresponding to the **a** and **b** directions. The 2-D network can be described as a succession of Fe_4 perfect rectangles, which diagonals are close to the Fe-Pt-Fe bridges (Figure 2). Following the notation of reference 30, these Fe_4 rectangles are called pseudo-squares hereafter. As NC-Pt-CN bridges are a little longer than the rectangle diagonals, the CN branches of $[Pt(CN)_4]^{2-}$ moieties lie slightly out of the Fe_4 plane, leading to a slight corrugation of the 2D layers. The FeN_4 planes are tilted from the $Pt(CN)_4$ planes by 7.46(8)° and 8.30(8)° at 296 K and 110 K, respectively (Figure 3). In addition to the direct interactions through the NC-Pt-CN bridges, the elastic connection between the iron centers within the 2D planes is assisted by a direct H-bond interaction between a C-H from the triazole moiety and the OH group of an adjacent ligand and by indirect significant H-bonding *via* the water molecules between two triazole within the **a** direction (Figure 3 and table 3).

The 2D layers are stacked and interdigitated along the **c** direction, connected to each other by interlayer π-stacking interactions between the triazole moiety and the phenyl groups of 3phOH-trz ligands of successive layers along the **b** direction (Figure 4). Additionally, H-bonds between the hydroxyl group and

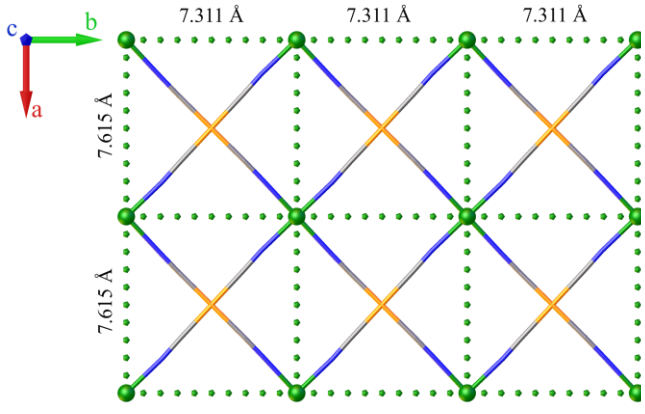

Figure 2. View of the 2D arrangement of **2** at 296 K: projection along the **c** direction showing the Fe_4 pseudosquares.

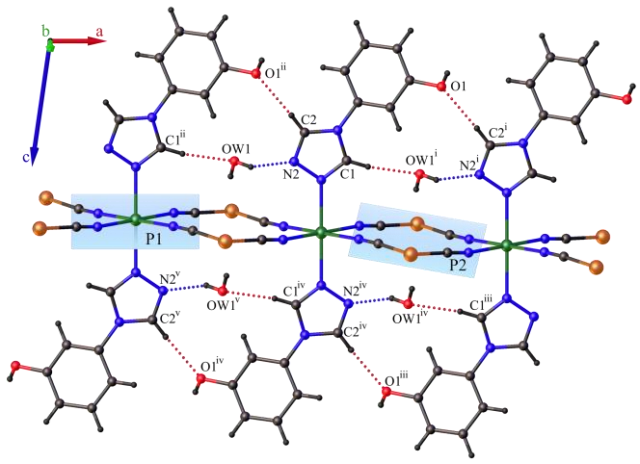

Figure 3. View along the [0, 1, 0] direction at ambient temperature showing the FeN_4 equatorial plane slightly tilted with respect to the $[Pt(CN)_4]^{2-}$ plane (P1-P2 angle = 7.46(8)°). [i]1+x,y,z ; [ii]-1+x,y,z ; [iii]2-x,2-y,1-z ; [iv]1-x,2-y,1-z ; [v]-x,2-y,1-z

Table 2. Selected bond lengths and distortion parameters of the coordination sphere of compound **2**.

Atoms	distance / Å			
	296 K HS	110 K HS	10 K HS	10 K LS*
Fe1-N1	2.197(2)	2.191(2)	2.187(2)	1.989(2)
Fe1-N4	2.158(3)	2.137(2)	2.142(2)	1.936(2)
Fe1-N51	2.152(3)	2.148(2)	2.140(2)	1.944(2)
<Fe1-N>	2.169(3)	2.159(2)	2.157(2)	1.956(2)
	Distortion / °			
[a]Σ (°)	24(1)	26(1)	27(1)	22(1)
[b]Θ (°)	59(2)	62(2)	72(2)	57(2)

[1]1-X,1-Y,1-Z ; [a]Σ is the sum of the deviation from 90° of the 12 cis-angles of the FeN_6 octahedron[35]; [b]Θ is the sum of the deviation from 60° of the 24 trigonal angles of the projection of the FeN_6 octahedron onto its trigonal faces.[35]

Table 3. Intermolecular interactions of compound **2** (Å, °)

T / spin state	293 K / HS			110 K / HS			10 K / HS			10 K / LS		
H-bonds interaction												
D-H⋯A	**d(H-A)**	**d(D-A)**	**D-H-A**	**d(H-A)**	**d(D-A)**	**D-H-A**	**d(H-A)**	**d(D-A)**	**D-H-A**	**d(H-A)**	**d(D-A)**	**D-H-A**
C2-H2⋯O1[2]	2.32	3.250(5)	177	2.29	3.219(4)	176	2.28	3.207(3)	176	2.24	3.172(3)	177
C1 H1⋯OW1[1]	2.26	3.180(4)	170	2.25	3.176(3)	171	2.26	3.180(3)	172	2.22	3.105(3)	159
OW1-HW1A⋯N2	2.01	2.778(4)	157	1.93	2.761(3)	165	1.94	2.756(3)	160	1.92	2.719(3)	163
O1-H1A⋯OW1[3]	1.95	2.745(4)	172	1.91	2.723(4)	171	1.91	2.721(3)	172	1.87	2.687(3)	171
π-stacking interactions												
Planes	**angle[a]**	**distance[b]**	**shift[c]**	**angle[a]**	**distance[b]**	**shift[c]**	**angle[a]**	**distance[b]**	**shift[c]**	**angle[a]**	**distance[b]**	**shift[c]**
plane1 / plane2[4]	5.261	3.973	1.710	5.426	3.955	1.712	5.324	3.936	1.701	4.321	3.813	1.615
plane1 / plane2[3]	5.261	3.660	1.081	5.426	3.622	1.045	5.324	3.614	1.033	4.321	3.579	1.313

[1]1+X,+Y,+Z; [2]-1+X,+Y,+Z; [3]1-X,1/2+Y,1/2-Z ; [4]1-X,-1/2+Y,1/2-Z ; [a]Angle between planes ; [b]Centroid-Centroid distance ; [c]Shift distance ; Plane1=C3C4C5C6C7C8 ; Plane2=N1C1N3C2N2.

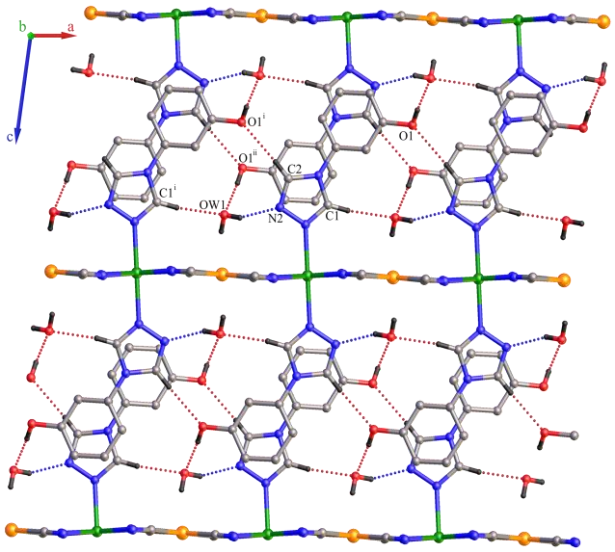

Figure 4. 3D crystal packing of **2** at ambient temperature along the [0, 1, 0] direction showing the intermolecular interactions and the quasi inexistent corrugation. [i]-1+x,y,z ; [ii]1-x,-½+y,½-z

a triazole moiety of an adjacent ligand link the layers along the **b** direction *via* the water molecules. Both interactions ensure the interlayer network cohesion within the **c** direction.

It is worth to note that the longest Fe-Fe distance (7.6149(2) Å at 293 K and 7.6230(2) Å at 110 K) of the Fe_4 rectangles correspond to the intra-layer H-bonding interactions direction, whereas the shortest ones (7.3105(2) Å at 293 K and 7.2775(2) Å at 110 K) to the inter-layer π-stacking interactions (figures 2, 3 and 4). Due to the *trans* position of the hydroxyl group with respect to the free N atom of the triazole on the 3phOH-trz ligand, the water molecules are connected on both side of the ligand by H-bonding interactions leading to a symmetrical distribution of the solvent molecules around the ligands. These two latter observations constitute the main differences in the local crystal structure compared to compound **1**, $[Fe(2\text{-pytrz})\{Pt(CN)_4\}].3H_2O$[30]. This parent compound displays two different Fe(II) centers leading to two different FeN_6 environments for which only one of them exhibits a thermal SCO behaviour, while in compound **2**, the crystal structure is built from only one iron(II) center. Moreover, **1** shows a different interactions network where water molecules were all located on the same side of the ligand, leading to an asymmetric distribution of the solvent molecules around the ligand. Additionally, no direct or indirect interactions were found between the ligands within the same layer, conversely to what is observed in **2**. These observations explain (i) why the corrugation of the 2D network is much less pronounced in this case as the symmetrical distribution of the water molecules prevent the tilt of one iron center and (ii) why the pseudo-squares observed in the parent compound are much more distorted in **2** to reach a rectangular geometry as the presence of significant interactions between ligands in the same layer impose a longer distance within the **a** direction (Tables SI1 and SI2). These observations lead us to predict a paramagnetic behavior or a complete one-step SCO transition.

The coordination sphere around the Fe atom remains almost unchanged at 296 K and 110 K and adopts a slightly distorted octahedral geometry involving an FeN_4 equatorial plane arising from four nitrogen atoms of the $[Pt(CN)_4]^{2-}$ anions and two N atoms in axial positions from the 3phOH-trz ligands. The mean Fe-N bond length – 2.169 Å and 2.159 Å at 296 K and 110 K respectively – range close to those expected for a iron(II) cation in the HS state. The octahedron distortion is small for a HS iron(II) at both temperatures as is usually observed for "Hoffman like" spin crossover compounds (table 2).[33] Nevertheless the present octahedron distortion is more pronounced than other 2D SCO "Hoffman like" compounds[34]. Interestingly, compared to the parent compound **1**, the iron site distortion is closer to the Fe2 site that did not undergo the thermal spin transition and higher than those observed for the others hydrated triazole-based 2D SCO Hofmann-like networks.[29]. Paez-Espejo *et al.*[26] introduced an elastic model to explain the conditions of occurrence of multistep transitions in 2D spin crossover solids, as a function of a frustration parameter ξ. For the present compound (**2**), the frustration parameter ξ can be evaluated slightly higher than that calculated for **1** (ξ ~ 0.2 for **2** and ~ 0.1 for **1**) or identical if the model chosen in the case of compound **2** is rectangular (ξ ~ 0.1). For such ξ values one-step transitions are expected in both cases. However, it was already suggested that the additional square distortion (square distortion Sd of the pseudo-squares as defined in legend of table 4) should play a significant role on the spin transition leading to a two-step transition for the parent compound.[30] It possibly precludes here the SCO of the compound **2** as the "pseudo-square" around the iron site is strongly distorted. Using the same parameter Sd[30] the square distortion of compound **2** appears high at 296 K and increases at 110 K. This value is significantly higher than the

value obtained for **1** (table 4) and is always greater than those observed for others hydrated triazole based 2D "Hoffman like" compounds except in case of the $[Fe^{II}Pd\text{-}(CN)_4(thiome)_2]\cdot 2H_2O$ (thiome = 4-[(*E*)-2-(5-methyl-2-thienyl) vinyl]-1,2,4-triazole)[29d] derivative that does not undergo any SCO on the whole studied temperature range. This higher distortion of compound **2** could result in stronger elastic frustration that may quench the spin transition in the present case. It seems that square distortion greater than 4-5 %, also linked to higher iron octahedron deformation, could preclude the spin transition on the corresponding site. It is worth noting that, within this family, when several iron sites are present, the less distorted site undergoes the SCO firstly when cooling down, leading to an increase of the square distortion of the second site. When this distortion becomes too high, the SCO may be quenched on the second site as it is observed for compound **1**.

Table 4. Fe···Fe and Pt···Pt distances (Å) and squares distortion (Sd, %) in the pseudosquares within the 2D layers

	293 / HS	**110K / HS**	**10K / HS**	**10K / LS**
	distance / Å			
Fe…Fe[a]	7.6149(2)	7.6230(2)	7.6326(3)	7.4562(3)
Fe…Fe[b]	7.3105(2)	7.2775(2)	7.2627(3)	6.8994(3)
Pt…Pt[a]	7.6149(2)	7.6230(2)	7.6326(3)	7.4562(3)
Pt…Pt[b]	7.3105(2)	7.2775(2)	7.2627(3)	6.8994(3)
Sd[c]	0.042	0.047	0.051	0.081

[a]within the (100) crystallographic direction, [b]within the (010) crystallographic direction, [c]Sd is defined as the difference of both sides of the pseudosquare around Fe divided by the shortest side of the pseudo squares. This definition gives $Sd = |d(Pt\cdots Pt^a) - d(Pt\cdots Pt^b)|/d(Pt\cdots Pt^b)$.

Magnetic and photomagnetic properties.

The magnetic properties of **2** were measured on a polycrystalline sample from 300 K to 10 K. Figure 5 reports the thermal evolution of $\chi_M T$ where χ_M is the magnetic molar susceptibility and T the temperature. At 300 K, the $\chi_M T$ value of 3.96 cm^3 K mol^{-1} is consistent with a HS iron(II) ion with a g value of 2.3. Upon cooling, the $\chi_M T$ product remains almost constant down to 50 K. Below this temperature a faster decrease is observed, probably due to the zero-field splitting of the paramagnetic iron(II) ion.[36] This behavior is completely reversible upon warming. The absence of SCO behavior for **1** fulfils to our goal that was to inhibit it by elastic strains. Compare to the compound from Sciortino *et al.*[29a] that reported a 4-steps SCO using a phenol substituted triazole ligand, the absence of any SCO in **2** could be explained by a more rigid ligand used in our case.

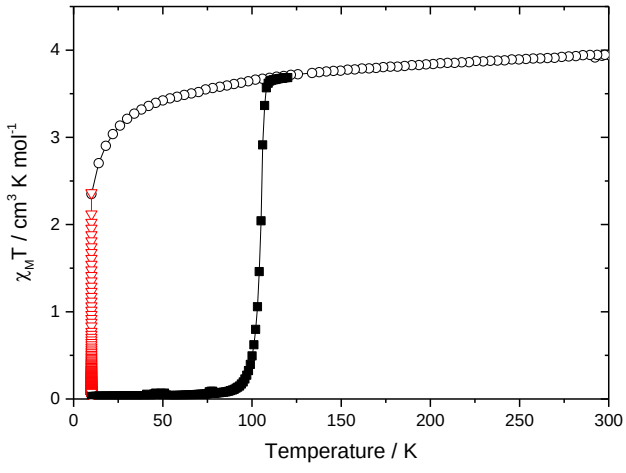

Figure 5: Thermal dependence of $\chi_M T$ before light irradiation (o) during irradiation at 830 nm (∇) and after irradiation (■) upon heating at 0.4 K/mn in the dark.

The reverse-LIESST effect was then attempted on the sample using a 830 nm irradiation. Figures 5 and 6 report the experiment performed at 10 K. A decrease of $\chi_M T$ is recorded upon irradiation down to 0.04 cm^3 K mol^{-1} after one hour indicating a fully efficient reverse-LIESST in a relatively short time. From the generated photo-induced LS state, two experiments can then be performed.

The first one that can be performed is the photocycling of the sample. From the LS state, an irradiation at 510 nm induces the complete population of the HS state in less than one hour (Figure 6). The photoswitching properties of this material are then reversible, reaching at each step the fully saturated LS and HS states. In addition, the photoswitching time appears equivalent for the LIESST and the reverse-LIESST processes, which is unusual. Finally, the HS populated by a 510 nm irradiation exhibits the same paramagnetic behavior than the pristine compound.

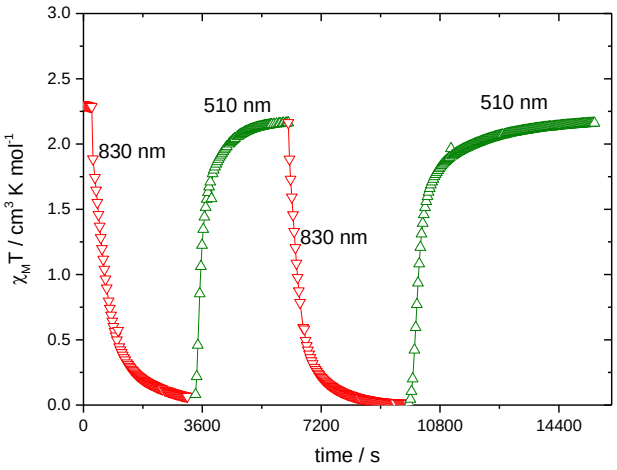

Figure 6: Photocycling of the sample **2** upon alternative irradiation at 830 nm (∇) and 510 nm (Δ).

The second experiment to be performed is to check the magnetic behavior of the photo-induced LS state. After red light irradiation, the light was switched off and the temperature was increased at 0.4 K/mn up to 120 K. Figure 5 clearly shows an abrupt LS to HS spin transition with a $T_{1/2}$ of 105 K. In a certain way, this opens a 105 K large hysteresis since upon cooling the system remains HS. By analogy to other examples,[23,30,37] this curve should reflect the spin crossover behavior of the LS state. This behavior is only accessible by light irradiation since the HS state exhibits an extremely long lifetime. This can be evidenced by a comparison of the time dependence of $\chi_M T$ at 50 K with and without irradiation (Figure SI5). During seven hours in the dark, the system retains its HS state, without any evidence of signal decrease while in two hours of irradiation at 830 nm, the fully LS state is populated. This observation can be compared to the pressure-induced SCO phenomenon that has been observed in the $[Fe^{II}Pd\text{-}(CN)_4(thiome)_2]\cdot 2H_2O$[29d] that goes from HS to a complete 2-steps SCO under pressure.

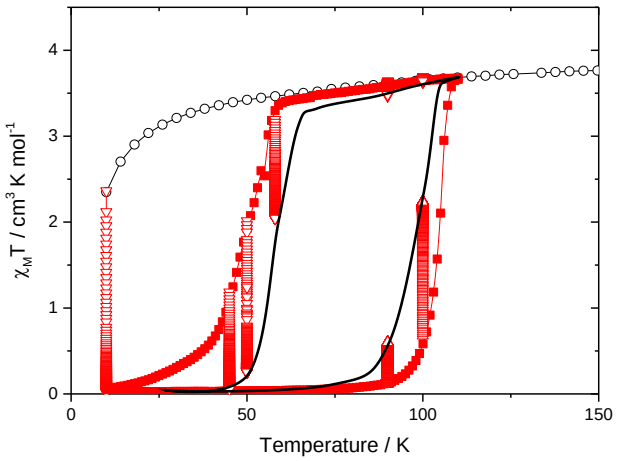

Figure 7: Thermal dependence of $\chi_M T$ under permanent light irradiation at 830 nm (■). The up and down red triangles stand for the isothermal kinetics of the HS fraction under light recorded at different temperatures in order to drawn the envelope of the quasi-static LITH loop (black curve) made of photostationnary states.

The long-lived HS state lets us to suspect the presence of a hidden hysteresis loop whose upper branch would correspond to the measured LS → HS transition curve. To probe the existence of this hysteresis loop we have performed the LITH measurements.[19a,38] This approach was used to reveal the hidden hysteresis in **1**.[30] Upon constant light irradiation at 830 nm, the sample is heated from the photoexcited LS state at 10 K to the HS state at 110 K and then cooled down at 0.4 K/mn. It results in a non-equilibrium competition between the light-assisted population of the LS state and the thermal cooperative population of the HS state through the thermally induced spin crossover.

The LITH experiment of **2** is depicted in figure 7. It clearly shows the presence of a thermal hysteresis loop of 55 K width. Since such hysteresis is the result of an equilibrium between two antagonist pathways, it is very sensitive to the measurement timescale (temperature sweeping rate).[38,39] To have access to the true equilibrium (or the quasi-static) curve, several photostationary points were recorded at several temperatures along the cooling and warming branches. Under light irradiation, the temperature was set at the desired value, and the temporal evolution of $\chi_m T$ under light was recorded. This procedure led to reach the photo-stationary states, from which an envelope of the quasi-static LITH loop (black curves) of 37 K width can be drawn.

The photostationary points at 100 K (Figure SI6) are illustrative of the presence of a bistable region under light irradiation: from the pure LS state $\chi_M T$ reaches a value of 2.18 cm^3 K mol^{-1} while it remains constant at 3.64 cm^3 K mol^{-1} from the cooling branch. This bistable region spreads itself over 37 K.

Regarding the quasi-static LITH, the warming branch under irradiation in figure 7 is close to the warming branch without irradiation (see Figure 5). This weak difference strengthens the argument that the heating branch of the reverse-LITH curve describes the thermally-induced spin transition of a hidden stable LS state towards the HS phase around 100 K. On cooling from the HS state, near-infrared irradiation favored the occurrence of the reversible HS→LS transition around 55 K. This closed thermal hysteresis loop is related to the transition of iron center, while in the dark the system stays trapped in the HS state. This reveals the presence of a hidden thermal hysteresis which was not accessible by classical thermal ways.

Recently, a 2D paramagnetic {[Fe(bbtr)$_3$](BF$_4$)$_2$} sample was evidenced to exhibit a hidden hysteresis revealed by reverse-LIESST effect as well as a light-induced bistability using selective wavelengths.[40] The hidden hysteresis curve was suspected from the presence of an instability curve, typical of hysteretic systems. The experimental envelop of this hysteresis was, however, not recorded, and a crystallographic phase transition was evidenced. With our current study, we produce a new example with bidirectional selective photoswitching in the class of rare materials exhibiting this behavior, and overall we give chemical tools to promote such effects: elastic frustration is a parameter on which chemist can play to tune the properties of the resulting materials.

Photocrystallographic investigation.

In order to relate the frustration to a possible structural phase transition, photo-crystallographic experiments have been performed to explore the structural properties of **1** at 10K before and after irradiation at 850 nm. In both cases no crystallographic phase transition was observed and **1** crystallizes in the same system and space group than at room temperature, the crystal structure can then be described in the same way. At 10K after irradiation the unit cell volume decreases by 90 Å^3, which represents ca. 7.4 % of the unit cell volume before irradiation suggesting a HS to LS transition of the Fe cation. The FeN$_6$ geometry is significantly affected by the light irradiation. The mean Fe-N distances decrease from 2.157(2) Å before irradiation to 1.956(2) Å after with a more regular octahedral geometry (table 2). It evidences a full HS to LS transition by the reverse-LIESST process. At 10K in the HS state the distortion of the "pseudo-squares" geometry (Sd = 5.1%) is higher than those at 110 K and 296 K (table 4), which confirms that the distortion increases when the temperature is cooled down. The difference between the nature of the interactions within the **a** and **b** directions (strong intra-layer H-bonding in the a direction and essentially interlayer π-stacking in the b direction) may explain this anisotropic structural behavior. The intermolecular interactions are significantly affected by the light induced HS to LS transition at 10K whereas their modifications due to the temperature variation (296K to 10K in the HS state) are comparatively small, especially concerning the H-bond intra-layer network (table 3). These modifications, in addition to the change of the spin state, lead to a more distorted pseudo-squares at 10K in the LS state (Sd = 8.1%), that should increase the elastic frustration of the lattice.

Conclusions

A new Hoffman-type two-dimensional network [Fe(3phOH-trz){Pt(CN)$_4$}].2H$_2$O was synthesized specifically to promote a strong hydrogen bonds network that we previously suspected to be responsible of the inhibition of the SCO behaviour. This effect was here confirmed, leading to a completely paramagnetic compound that remains HS down to 10 K. This compound consists of iron centers covalently linked by [Pt(CN)$_4$]$^{2-}$ anions giving a 2D coordination polymer within slightly corrugated layers formed by a succession of Fe$_4$ perfect rectangles. Compared to the parent [Fe(2-pytrz){Pt(CN)$_4$}].3H$_2$O compound **1**, the elastic frustration is higher in **2**, leading to a complete inhibition of the spin crossover. From the HS state, the reverse-LIESST process was applied to populate the fully LS state at 10 K. Upon near infrared irradiation

no particular structural changes occurred (except the usual unit cell volume change) and the network remained always constituted of one iron(II) crystallographic site. This LS state can be converted back to the HS state through a green light irradiation (510 nm) or upon warming. Indeed, heating in the dark the photo-induced LS state revealed a thermal LS to HS transition at 105 K. When the near infrared irradiation (830 nm) is applied while the sample is thermally cycled, a hidden hysteresis loop of 37 K width is revealed with an upper transition temperature equal to that of the dark process, suggesting that the LS state might be the true thermodynamically stable state of the system. This study evidences that the constraints brought by the water molecules network leads to a strong elastic frustration that inhibits the spin crossover behaviour.

This complete structure-property relationship study gives important insights on the role of elastic frustration on the level of inhibition of the spin crossover. This gives important trends to target wavelength selective photoswitching between two stable states, which is highly favourable compared to the current LIESST process that involves a metastable state with a given lifetime.

Experimental Section

Methods. The starting materials 1,2-diformylhydrazine, aminophenol and iron(II) perchlorate hydrate were purchased from Sigma Aldrich and used without further purification. Solvents were used and purified by standard procedures. IR spectra were obtained with a Vertex 70 BRUKER spectrometer equipped with a platinum ATR accessory. NMR spectra were recorded on a Bruker Advance 400 MHz, J values are given in Hz.

Syntheses

4-(3-hydroxyphenyl)-1,2,4-triazole (L1). 4-(3-hydroxyphenyl)-1,2,4-triazole has been synthesized according to the procedure previously published by Elokhina *et al*.[41] The reaction was carried out under nitrogen atmosphere. 1,2-diformylhydrazine (3.0g, 34 mmol.) and aminophenol (3.75g, 34 mmol.) with a small amount of hydroquinone were heated at 170°C for 30 mn. Then, the mixture was cooled down to 70°C, 20 mL of freshly distilled ethanol was further added and the mixture was stirred for 5 mn. It was then cooled down to 20°C and a volume of 100 mL of diethylic ether was added. The mixture was then kept at -20°C overnight. The crude product was collected after filtration as a dark brown powder, washed with ether and dried under vacuum. (yield 2.93g, 18 mmol, 53 %). ^{1}H NMR ($(CD_3)_2SO$), 400 MHz) δ: 6.84 (dd, 1H, $^{3}J_{H-H}$ = 2.4 Hz, $^{3}J_{H-H}$ = 2Hz), 7.04 (m, 2H), 7.17 (t, 1H, $^{3}J_{H-H}$ = 8 Hz), 9.05 (s, 2H), 10.05 (broad, 1H) ppm. ^{13}C NMR ($(CD_3)_2OD$, 75 MHz) δ: 110.06, 112.55, 113.63, 132.02, 136.20, 143.15, 160.36. ν(cm^{-1}): 3106(w), 3064(w), 2965(w), 2861(w), 2838(w), 2727(w), 2662(w), 2627(w), 1667(m), 1598(s), 1529(s), 1493(s), 1389(m), 1287(s), 1248(m), 1203(s), 1164(m), 1091(m), 1030(w), 995(w), 860(s), 831(w), 783(s), 685(s), 645(w), 607(m), 553(m), 504(m), 467(w), 458(m).

$[Fe(3phOH\text{-}trz)_2\{Pt(CN)_4\}].2H_2O$. The ligand **L1** (20 mg, 0.10 mmol.) was solubilized in 10 mL of dry ethanol. A solution of potassium tetracyanoplatinate (26 mg, 0.06 mmol.) in 5 mL of water was slowly poured into this solution. The mixture was stirred at r.t. for 15 mn. 2 mL of this solution was then transferred into a thin glass tube. Next, a freshly prepared aqueous solution (6 mL) of $Fe(ClO_4)_2$, $6H_2O$ (15 mg, 0.01 mmol.) was slowly layered on the top of the tube for slow diffusion. After several days, thin colorless plates appeared at the interface and were collected in an amount sufficient for the structural and physical studies. Anal. Calcd for $C_{20}H_{18}FeN_{10}O_4Pt$: C, 33.7; H, 2.5; N, 19.6 %. Found: C, 33.5; H, 2.6; N, 19.4 %. IR (ATR), ν(cm^{-1}): 3620(w), 3186(w), 3115(w), 2992(w), 2169(s), 1599(s), 1531(s), 1494(s), 1366(w), 1278(s), 1241(w), 1211(s), 1167(w), 1096(m), 1043(m), 1006(w), 981(w), 899(w), 869(s), 858(s), 778(s), 669(s), 600(w), 533(w), 500(w), 478(w), 454(m).

Magnetic and Photomagnetic Studies.

Magnetic susceptibility data were collected using a Quantum Design MPMS 5 SQUID magnetometer under an applied field of 1 T. All measurements were performed on homogenous polycrystalline samples and in the temperature range 10 to 290 K. Diamagnetic corrections for the sample holder and the material (using Pascal constants) were applied.
Photomagnetic measurements were performed with a set of photo-diodes coupled through an optical fiber to the cavity of a MPMS-55 Quantum Design SQUID magnetometer operating at 2 T. The intensity of irradiation was set to prevent heating of the sample. The crystalline sample was prepared in a thin layer (0.66 mg) to promote full penetration of the irradiated light. Our previously published standardized method for obtaining LIESST data was followed.[19,20] The sample was first slow cooled to 10 K, ensuring that potential trapping of HS species at low temperatures did not occur. Irradiation was carried out at a set wavelength and the power at the sample surface was adjusted to 5 mW cm^{-2}. Once photo-saturation was reached, irradiation was ceased and the temperature increased at a rate of 0.4 K.min^{-1} to ~100 K and the magnetization measured every 1 K to determine the T(LIESST) value given by the extreme of the $\delta \chi_M T / \delta T$ versus T curve for the relaxation. The T(LIESST) value describes the limiting temperature above which the light-induced magnetic high-spin information is erased in a SQUID cavity. In the absence of irradiation, the magnetism was also measured over the temperature range 10 – 290 K to follow the thermal spin transition and to obtain a low temperature baseline.

Crystallographic and photo-crystallographic investigations:

Single crystal X-ray studies were performed at 296 K and 110 K on Xcalibur 2 κ-CCD diffractometer using Mo Kα radiation (λ = 0.71073 Å). The corresponding structures were solved by direct methods with the SHELXS program and refined on F^2 by weighted full matrix least- squares methods using the SHELXL program.[42]. All non-hydrogen atoms were refined anisotropically, hydrogen atoms were located in difference Fourier maps and treated using a riding model. Crystallographic data and refinement details are provided in Table 1.

10K single crystal diffraction data were collected on a Microfocus Supernova diffractometer equipped with a two dimensional ATLAS detector, using Mo Kα radiation, and a Helijet He open flow cryosystem. In situ photo-excitations were carried out using a 850 nm diode laser (duration 10 min), until the photo-stationary state was reached to populate the LS state by reverse-LIESST. The single crystal sample was rotated continuously during excitation to ensure a homogeneous and complete excitation. The corresponding structures were solved by direct methods with the SHELXS program and refined on F^2 by weighted full matrix least-squares methods using the SHELXL program. All non-hydrogen atoms were refined anisotropically, hydrogen atoms were located in difference Fourier maps and treated using a riding model.
CCDC 1574585-1574588 contain the supplementary crystallographic data. These data can be obtained free of charge from The Cambridge Crystallographic Data Centre via www.ccdc.cam.ac.uk/data_requ- est/cif.

Acknowledgments

We thank the CNRS, the Universities of Brest, Paris-Saclay Lorraine, Versailles and Bordeaux, the "Agence Nationale de la Recherche" (ANR project BISTA-MAT: ANR-12-BS07-0030-01) and “Région Nouvelle Aquitaine” for the funding of this work.

[1] a) J. M. Lehn, *Science* **2002**, 295, 2400; b) M. Ruben, U. Ziener, J. M. Lehn, V.Ksenofontov, P. Gütlich, G. B. M. Vaughan, *Chem. Eur. J.* **2005**, 11, 94; c) M. Fujita, D. Oguro, M. Miyazawa, H. Oka, K. Yamaguchi, K. Ogura, *Nature* **1995**, 378, 469; d) O. M. Yaghi, M. O’Keeffe, N. W. Ockwig, H. K. Chae, M. Eddaoudi, J. Kim, *Nature* **2003**, 423, 705.

[2] E. Breuning, M. Ruben, J. M. Lehn, F. Renz, Y. Garcia, V. Ksenofontov, P. Gütlich, E. Wegelius, K. Rissanen, *Angew. Chem.* **2000**, 112, 2563; *Angew. Chem. Int. Ed.* **2000**, 39, 2504.

[3] Spin Crossover in Transition Metal Compounds I−III. In Topics in Current Chemistry; P. Gütlich. H-A. Goodwin., *Eds.; Springer-Verlag: Berlin, Germany*, **2004**; Vols. 233−235.

[4] K. Nasu, *Photoinduced Phase Transitions* (World Scientific, 2004)

[5] H. Cailleau, T. Luty, S. Koshihara, M. Servol, M. Lorenc, M. Buron-Le Cointe, E. Collet, *Acta Phys. Polon. A* **2012**, *121*, 297.

[6] M. Chergui, E. Collet, *Chem. Rev.*, **2017**, *117*, 11025.

[7] A. Bousseksou, G. Molnar, L. Salmon, W. Nicolazzi, *Chem. Soc.Rev*, **2011**, 40, 3313.

[8] O. Kahn, C.J. Martinez, Science **1998**, 279, 44**.**

[9] P. Gütlich, A. B. Gaspar, Y. Garcia, Beilstein J. Org. Chem. **2013**, 9, 342.

[10] a) L. Cambi, L.Szego, *Chem. Ber. Dtsch. Ges.* **1931**, 64, 2591. b) P.L Franke, J.G Haasnoot, A. P Zuur, *Inorg. Chim. Acta* **1982**, 59, 5.

[11] P. Gütlich, A. Hauser, H. Spiering, *Angew. Chem., Int. Ed. Engl*. **1994**, 33, 2024.

[12] a) M.-L. Boillot, J. Zarembowitch, A. Sour, *Top. Curr. Chem*. **2004**, *234*, 261; b) C. Roux, J. Zarembowitch, B. Gallois, T. Granier, R. Claude, *Inorg. Chem.* **1994**, *33*, 2273; c) M.-L. Boillot, C. Roux, J.-P. Audière, A. Dausse, J. Zarembowitch, *Inorg. Chem*. **1996**, *35*, 3975.

[13] a) K. Senechal-David, N. Zaman, M. Walko, E. Halza, E. Rivière, R. Guillot, B.L. Feringa, M.-L. Boillot, *Dalton Trans*. **2008**, 1932; b) Y. Garcia, V. Ksenofontov, R. Lapouyade, A.D. Naik, F. Robert, P. Gutlich, *Opt. Mater*. **2011**, *33*, 942; c) M. Nihei, Y. Suzuki, N. Kimura, Y. Kera, H. Oshio, *Chem. Eur. J.* **2013**, *19*, 6946; d) M. Milek, F.W. Heinemann, M.M. Khusniyarov, *Inorg. Chem*. **2013**, *52*, 11585; d) B. Rosner, M. Milek, A. Witt, B. Gobaut, P. Torelli, R.H. Fink, M.M. Khusniyarov, *Angew. Chem. Int. Ed. Engl*. **2015**, *54*, 12976.

[14] a) E. Freysz, S. Montant, S. Létard, J.-L. Létard, *Chem. Phys. Lett*. **2004**, *394*, 318 ; b) S. Bonhommeau, G. Molnar, A. Galet, A. Zwick, J.A. Real, J.J. McGarvey, A. Bousseksou, *Angew. Chem. Int. Ed. Engl*. **2005**, *44*, 2.

[15] M. Castro, O. Roubeau, L. Pineiro-Lopez, J. A. Real, J. A. Rodriguez-Velemazan, *J. Phys. Chem. C*. **2015**, *119*, 17334.

[16] a) S. Decurtins, P. Gütlich, C.P Kohler, H. Spiering, A. Hauser, *Chem. Phys. Lett*. **1984**, 105, 1 ; b) S. Decurtins, P. Gütlich, K.M Hasselbach, A. Hauser, H. Spiering, *Inorg. Chem.* **1985**, 24, 2174; c) A. Hauser, *Chem. Phys. Lett*. **1986**, 124, 543; d) A. Hauser, *Top. Curr. Chem*, **2004**, 234, 155.

[17] a) A. Hauser, *Coord. Chem. Rev*, **1991**, 111, 275; b) J. Jeftic, A. Hauser, J. *Phys. Chem. B*, **1997**, 101, 10262; c) H. Romstedt, A. Hauser, H. Spiering, *J. Phys. Chem. Solids*, **1998**, 59, 265; d) A. Vef, U. Manthe, P. Gutlich, A. Hauser, *J. Chem. Phys*, **1994**, 101, 9326.

[18] E. Buhks, G. Navon, M. Bixon, J. Jortner, *J. Am. Chem. Soc*, **1980**, 102, 2918.

[19] a) J.-F. Létard, P. Guionneau, L. Rabardel, J. A. K. Howard, A. E. Goeta, D. Chasseau, O. Kahn, *Inorg. Chem.* **1998**, 37, 4432 ; b) J.-F. Létard, L. Capes, G. Chastanet, N. Moliner, S. Létard, J. A. Real, O. Kahn, *Chem. Phys. Lett.* **1999**, 313, 115

[20] a) J. F. Létard, *J. Mater. Chem.* **2006**, 16, 2550; b) J. F. Létard, P. Guionneau, O. Nguyen, J. Sanchez Costa, S. Marcén, G. Chastanet, M. Marchivie, L. Goux-Capes, *Chem. Eur. J.* **2005**, 11, 4582; c) S. Marcen, L. Lecren, L. Capes, H. A. Goodwin, J.-F. Létard, Chem. Phys. Lett. **2002**, 358, 87; d) N. Shimamoto, S.-S. Ohkoshi, O. Sato, K. Hashimoto, *Inorg. Chem.* **2002**, 41, 678; e) J.-F. Létard, G. Chastanet, P. Guionneau, C. Desplanches, in Spin Crossover Materials: Properties and Applications, *Ed. Malcom A. Halcrow*, **2013**, John Wiley & sons, 475.

[21] a) S. Hayami, Z.-Z. Gu, Y. Einaga, Y. Kobayashi, Y. Ishikawa, Y. Yamada, A. Fujishima, O. Sato, *Inorg. Chem*. **2001**, *40***,** 3240; (b) J. Sanchez Costa, P. Guionneau, J.-F. Létard, *J. Phys.: Conference Series*, **2005**, *21*, 67.

[22] a) N. Shimamoto, S.-S. Ohkoshi, O. Sato, K. Hashimoto, *Inorg. Chem.* **2002**, *41*, 678 ; b) R. Lebris, C. Mathonière, J.-F. Létard, *Chem. Phys. Lett.* **2006**, *426*, 380 ; c) D. Li, R. Clérac, O. Roubeau, E. Harte, C. Mathonière, R. Le Bris, S. M. Holmes, *J. Am. Chem. Soc.*, **2008,** *130*, 252.

[23] A. Hauser, *Chem. Phys. Lett*. **1986**, *124*, 6

[24] a) N. Paradis, G. Chastanet, J.-F. Létard, *Eur. J. Inorg. Chem*. **2012**, 3618 ; b) N. Paradis, G. Chastanet, F. Varret, J.-F. Létard, *Eur. J. Inorg. Chem*, **2013**, 968 ; c) N. Paradis, G. Chastanet, T. Palamarciuc, P. Rosa, F. Varret, K. Boukheddaden, J.-F. Létard, *J. Phys. Chem. C*, **2015**, 119, 20039.

[25] J.-F. Létard, G. Chastanet, H. Tokoro, S. Ohkoshi, *Curr. Inorg. Chem.* **2016**, *6*, 34

[26] M. Paez-Espejo, M. Sy, K. Bokheddaden, *J. Am. Chem. Soc*. **2016**, *138*, 3202.

[27] a) C. Baldé, W. Bauer, E. Kaps, S. Neville, C. Desplanches, G. Chastanet, B.Weber, J.-F. Létard, *Eur. J. Inorg. Chem*. **2013**, 2744 ; b) E. Trzop, D. Zhang, L. Pineiro-Lopez, F. J. Valverde-Munoz, M. Carmen Munoz, L. Palatinus, L. Guerin, H. Cailleau, J. A. Real, and E.Collet *Angew. Chem. Int. Ed.* **2016**, *55*, 8675.

[28] a) N. Pittala, F. Thétiot, S. Triki, K. Boukheddaden, G. Chastanet, M. Marchivie, *Chem. Mater.*, **2017**, *29*, 490 ; b) N. Pittala, F. Thétiot, C. Charles, S. Triki, K. Boukheddaden, G. Chastanet, M. Marchivie, *Chem. Commun.*, **2017**, *53*, 8356.

[29] a) N. F. Sciortino, K.A. Zenere, M.E. Corrigan, G.J. Halder, G. Chastanet, J.-F. Létard, C.J. Kepert, S.M. Neville, *Chem. Sci.* **2017**, *8*, 701; b) Y.M. Klein, N.F. Sciortino, F. Ragon, C.E. Housecroft, C.J. Kepert, S.M. Neville, *Chem. Commun.* **2014**, *50*, 3838 ; c) M.J. Murphy, K.A. Zenere, F. Ragon, P.D. Southon, C.J. Kepert, S.M. Neville, *J. Am. Chem. Soc*. **2017**, *139*, 1330; d) N.F. Sciortino, F. Ragon, K.A. Zenere, P.D. Southon, G.J. Halder, K.W. Chapman, L. Pineiro-Lopez, J.A. Real, C.J. Kepert, S. M. Neville, *Inorg. Chem*. **2016**, *55*, 10490.

[30] E. Milin, V. Patinec, S. Triki, E.-E. Bendeif, S. Pillet, M. Marchivie, G. Chastanet, K. Boukheddaden, *Inorg. Chem.* **2016**, *55*, 11652

[31] a) N. F. Sciortino, K.R. Scherl-Gruenwald, G. Chastanet, G.J. Halder, K.W. Chapman, J.-F. Létard, C.J. Kepert, *Angew. Chem. Int. Ed. Engl*. **2012**, *51*, 10154; b) F. Ragon, K. Yaksi, N.F. Sciortino, G. Chastanet, J.-F. Létard, D.M. D'Alessandro, C.J. Kepert, S.M. Neville, *Aust. J. Chem.* **2014**, *67*, 1563; c) N.F. Sciortino, S.M. Neville, J.-F. Letard, B. Moubaraki, K.S. Murray, C.J. Kepert, *Inorg. Chem*. **2014**, *53*, 7886; d) F.J. Valverde-Muñoz, M. Seredyuk, M.C. Muñoz, K. Znovjyak, I.O. Fritsky, J.A. Real, *Inorg. Chem.* **2016**, *55*, 10654; e) N.F. Sciortino, S.M. Neville, C. Desplanches, J.-F. Letard, V. Martinez, J.A. Real, B. Moubaraki, K.S. Murray, C.J. Kepert, *Chem. Eur. J.* **2014**, *20*, 7448. ; f) V. Niel, A.L. Thompson, A.E. Goeta, C. Enachescu, A. Hauser, A. Galet, M.C. Munoz, J.A. Real, *Chem. Eur. J.* **2005**, *11*, 2047; g) Y. Meng, Q.-Q. Sheng, M. Najbul Hoque, Y.-C. Chen, S.-G. Wu, J. Tucek, R. Zboril, T. Liu, Z.-P. Ni, M.-L. Tong, *Chem. Eur. J.* **2017**, *23*, 10034; h) V. Martinez, Z. Arcis Castillo, M.C. Munoz, A.B. Gaspar, C. Etrillard, J.-F. Letard, S.A. Terekhov, G. V. Bukin, G. Levchenko, J.A. Real, *Eur. J. Inorg. Chem*. **2013**, 813; i) T. Delgado, A. Tissot, C. Besnard, L. Guenée, P. Pattison, *Chem. Eur. J.* **2015**, *21*, 3664.

[32] a) M. C. Munoz, J.A. Real, *Coord. Chem. Rev*. **2011**, *255*, 2068; J.A. Real, A.B. Gaspar, M.C. Munoz, *Dalton Trans*. **2005**, 2062.

[33] a) R. Ohtani, M. Arai, H. Ohba, A. Hori, M. Takata, S. Kitagawa, M. Ohba, *Eur. J. Inorg. Chem*. **2013**, *2013*, 738; b) G. Agusti, M.C. Munoz, A.B. Gaspar, J.A. Real, *Inorg. Chem*. **2008**, *47*, 2552.

[34] (a) V. Martínez, A.B. Gaspar, M.C. Muñoz, G.V. Bukin, G. Levchenko, J.A. Real, *Chem. - A Eur. J.* **2009**, *15*, 10960. ; b) R. Ohtani, M. Arai, H. Ohba, A. Hori, M. Takata, S. Kitagawa, M. Ohba, *Eur. J. Inorg. Chem.* **2013**, 738. ; c) S. Sakaida, K. Otsubo, O. Sakata, C. Song, A. Fujiwara, M. Takata, H. Kitagawa, *Nat. Chem.* **2016**, *8*, 377. ; d) L. Pineiro-Lopez, M. Seredyuk, M.C. Munoz, J.A. Real, *Chem. Commun*. **2014**, *50*, 1833; e) R. Ohtani, M. Arai, A. Hori, M. Takata, S. Kitao, M. Seto, S. Kitagawa, M. Ohba, *J. Inorg. Organomet. Polym*. **2013**, *23*, 104 ; f) V. Niel, J. M. Martinez-Agudo, M.C. Munoz, A.B. Gaspar, J.A. Real, *Inorg. Chem*. **2001**, *40*, 3838 ; g) F.J. Munoz-Lara, A.B. Gaspar, M.C. Munoz, V. Ksenofontov, J.A. Real, *Inorg. Chem*. **2013**, *52*, 3; h) J.E. Clements, J.R. Price, S.M. Neville, C.J. Kepert, *Angew. Chem. Int. Ed. Engl*. **2016**, *55*, 15105 ; i) C. Bartual-Murgui, L. Salmon, A. Akou, N.A. Ortega-Villar, H.J. Shepherd, M. C. Munozz, G. Molnar, J.A. Real, A. Bousseksou, *Chem. Eur. J.* **2012**, *18*, 507.

[35] a) P. Guionneau, M. Marchivie, G. Bravic, J.-F. Létard, D. Chasseau, *Top. Curr. Chem.* **2004**, *234*, 97; b) M. Marchivie, P. Guionneau, J.-F. Létard, D. Chasseau, *Acta Cryst.* **2005**, *B61*, 25.

[36] O. Kahn, *Molecular Magnetism*, VCH, Weinheim, Germany, 1993

[37] R. Hinek, H. Spiering, P. Gütlich, A. Hauser, *Chem. Eur. J.* **1996**, *2*, 1435

[38] a) A. Desaix, O. Roubeau, J. Jeftic, J.G. Haasnoot, K. Boukheddaden, E. Codjovi, J. Linarès, M. Noguès, F. Varret, *Eur. Phys. J. B* **1998**, *6*, 183.; b) K. Boukheddaden, I. Shteto, B. Hôo, F. Varret, *Phys. Rev. B* **2000**, *6*, 14796; c) J. Jeftic, M. Matsarski, A. Hauser, A. Goujon, E. Codjovi, J. Linarès, F. Varret, *Polyhedron* **2001**, *20*, 1599; d) J.-F. Létard, G. Chastanet, O. Nguyen, S. Marcèn, M. Marchivie, P. Guionneau, D. Chasseau, P. Gütlich, *"Molecular Magnets Recent Highlights"*, Eds W. Linert & M. Verdaguer, Springer Wien N.-Y. **2003**, 49; e) C. Enachescu, R. Tanasa, A. Stancu, G. Chastanet, J.-F. Létard, J. Linares, F. Varret, *J. Appl. Phys*. **2006**, *99*, 08J504.

[39] a) R. Traiche, M. Sy, H. Oubouchou, G. Bouchez, F. Varret, K. Boukheddaden, *J. Phys. Chem. C.* **2017**, *121*, 11700; b) M. Sy, D. Garrot, A. Slimani, M. Paez-Espejo, F. Varret, K. Boukheddaden, *Angew. Chem. Int. Ed*. **2016**, *55*, 1755 –1759

[40] a) P. Chakraborty, R. Bronisz, C. Besnard, L. Guénée, P. Pattison, A. Hauser, *J. Am. Chem. Soc.* **2012**, *134*, 4049; b) P. Chakraborty, S. Pillet, E.-E. Bendeif, C. Enachescu, R. Bronisz, A. Hauser, *Chem. Eur. J.* **2013**, *19*, 11418.

[41] V. N. Elokhina, A. S. Nakhmanovich, *Russ. J. Gen. Chem*. **2006**, *76*, 158.

[42] a) Sheldrick, G. *Acta Crystallogr. Sect. C* **2015**, *71*, 3; b) Sheldrick, G. M. *Acta Crystallogr. Sect. A* **2008**, *64*, 112.

Received: ((will be filled in by the editorial staff))
Published online: ((will be filled in by the editorial staff))

Entry for the Table of Contents

Layout 1:

((Key Topic))

Hidden Hysteretic Behavior of a Paramagnetic Fe(II) Network Revealed by Light Irradiation

This paper reports the role of elastic frustration on the inhibition of spin crossover phenomenon, bringing the possibility to observe hidden hysteresis loop and selective wavelength bidirectional photoswitching between two stable states.

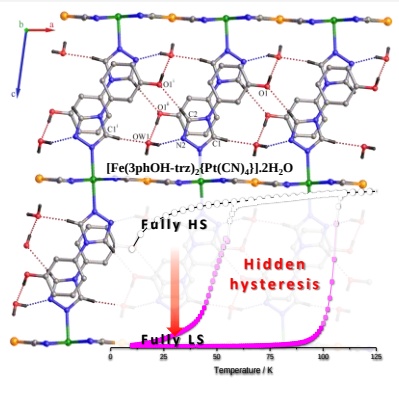

Mame Mguenar Ndiaye, Sébastien Pillet, El-Eulmi Bendeif, Mathieu Marchivie, Guillaume Chastanet, Kamel Boukheddaden, Smail Triki

…….. Page No. – Page No.

Keywords: Coordination Chemistry / Iron(II) / Spin-Crossover / LIESST / Photomagnetism / Hidden hysteresis / Elastic frustration